npj | 2D Materials and Applications

www.nature.com/npj2dmaterials

Correction: Publisher correction

REVIEW ARTICLE OPEN

Two-dimensional materials with piezoelectric and ferroelectric functionalities

Chaojie Cui[1], Fei Xue[2], Wei-Jin Hu[3] and Lain-Jong Li[2]

Two-dimensional (2D) layered materials with a non-centrosymmetric structure exhibit great potential for nano-scale electromechanical systems and electronic devices. Piezoelectric and ferroelectric 2D materials draw growing interest for applications in energy harvesting, electronics, and optoelectronics. This article first reviews the preparation of these functional 2D layered materials, including exfoliation methods and vapor phase deposition growth, followed by a general introduction to various piezo/ferro-electric characterization methods. Typical 2D piezoelectric and ferroelectric materials and their electronic properties, together with their potential applications, are also introduced. Finally, future research directions for 2D piezoelectric and ferroelectric materials are discussed.

npj 2D Materials and Applications (2018)2:18 ; doi:10.1038/s41699-018-0063-5

INTRODUCTION

Since the successful isolation of graphene by Novoselov et al. in 2004,[1] worldwide scientific efforts have been focused on wide range of two-dimensional (2D) layered materials, driven by the fundamental interest and their potential applications. Atomically thin 2D materials exhibit a wide range of unique electrical,[2,3] optical,[4,5] mechanical[6], and thermal[7] properties, which do not exist in their bulk counterparts, and the outstanding advantages of properties enlighten the development in light-weight and high-performance multifunctional applications.[8] Particularly, the 2D layered materials with non-centrosymmetric structure have great potential for nanoscale electromechanical systems and electronic device applications. Among them, piezoelectric and ferroelectric 2D materials have drawn a growing interest in recent years.[9–17]

The non-centrosymmetric material is an important research field because of the associated polarization and its potential application. Piezoelectricity is a property of electric polarization caused by macroscopic strains, a coupling between the mechanical and electrical behaviors to allow efficient mechanical-to-electrical energy conversion. Ferroelectricity is a property of spontaneous electric polarization that can be controlled by an applied external electric field. By now, a range of 2D layered materials have been experimentally confirmed or theoretically predicted as piezoelectric or ferroelectric,[10,13–15,18–28] like monolayer transition metal dichalcogenides (TMDCs) (such as MoS_2, $MoSe_2$, WS_2, and WSe_2),[10] group IV monochalcogenides (such as GeSe and SnS)[15,18–20] and group III–V binary compounds (such as AlSb, GaP, GaAs, InP, InAs, and InSb).[20–22] In section 2 we first summarize the synthetic methods of 2D materials, enumerating the preparation of some representative 2D materials as examples. Section 3 and 4, respectively, introduce typical 2D piezoelectric and ferroelectric materials and their electronic properties, together with their potential applications.

PREPARATION OF 2D MATERIALS AND THEIR PIEZO-/FERROELECTRIC CHARACTERIZATION METHODS

Two major strategies have been employed to obtain monolayer and few-layer 2D materials: one is the exfoliation of bulk crystals; the other is the direct growth through vapor phase deposition methods.

Preparation of 2D materials

Exfoliation methods. Exfoliation method is a top-down approach to prepare atomically thin 2D materials from the bulk crystals constructed by weak van der Waals interlayer interaction, which was applied to produce graphene in 2004.[1] In general, it can be realized by mechanical or chemical approaches.

Mechanical exfoliation, also called "Scotch tape method", is to prepare monolayer or few-layer 2D materials by applying an adhesive tape to cleave bulk crystals repeatedly.[29] This simple mechanical cleavage method has been used to successfully obtain a variety of 2D layered materials like graphene, boron nitride, dichalcogenides, and so on.[29] The as-prepared layered materials exhibit high crystallinity and clean surfaces, making them attractive for fundamental research. However, the obvious disadvantage of extremely low yield restricts its large-scale production and applications.

Regarding the chemical exfoliation, solvent-assisted exfoliation and ion intercalation assisted exfoliation are two typical approaches. Solvent-assisted exfoliation was proposed by Coleman et al. in 2011.[30] Many 2D layered materials (such as MoS_2, WS_2, $MoSe_2$, $MoTe_2$, BN, Bi_2Te_3, and so on) could be exfoliated from the bulk crystal counterparts by direct sonication in organic solvents like N-methylpyrrolidone (NMP) and isopropanol (IPA).[30,31] For the solvent assistance exfoliation process, selecting an appropriate solvent with a specific surface tension is critical because the energy of exfoliation could be minimized when the

[1]Department of Chemical Engineering, Tsinghua University, 100084 Beijing, China; [2]Physical Sciences and Engineering Division, King Abdullah University of Science and Technology, Thuwal, Jeddah 23955-6900, Saudi Arabia and [3]Shenyang National Laboratory for Materials Science, Institute of Metal Research (IMR), Chinese Academy of Sciences (CAS), Shenyang 110016, China
Correspondence: W-J. Hu (wjhu@imr.ac.cn) or L-J. Li (ljliv@tsmc.com)
These authors contributed equally: Chaojie Cui, Fei Xue.

Received: 24 February 2018 Revised: 21 May 2018 Accepted: 24 May 2018
Published online: 22 June 2018

surface energies of flake and solvent match well; therefore, an effective exfoliation could be successfully achieved.[30] Generally, solvents with the specific surface tension of ~40 mJ/m^2 are suitable for many materials (such as BN, MoS_2, and WS_2). Compared with mechanical exfoliation, the yield of the 2D material sheets by solvent assistance exfoliation could significantly increase. However, the practical application of this method is limted by the low dispersed concentration.

Ion intercalation method, the other way of chemical exfoliation, was first used in 1986 by Joensen et al.[32] to isolate individual MoS_2 sheets. The method is to widen the interlayer space by intercalated lithium, as well as the H_2 which evolves due to the reaction between water (or methanol, ethanol, and isopropanol) and intercalated lithium. By this method, monolayer MoS_2 sheets were successfully achieved. But this process usually requires a relatively high temperature and long reaction time (several days). Moreover, the 2H crystal structure of MoS_2 sheets usually becomes a mixture of 2H and 1T forms, and the low controllability of intercalation process leads to either a low yield of layered sheets with less intercalation, or decomposition of MoS_2 to metal nanoparticles and Li_2S with excess intercalation.[33]

The ion intercalation was improved later by introducing the concept of electrochemical process, which exploits a lithium foil as the anode and the objective layered bulk material, such as MoS_2, WS_2, or graphite, as the cathode to make a battery test cell (Fig. 1).[34,35] By in situ monitoring and adjusting the measurable galvanostatic discharge rates, the insertion content of Li can be accurately controlled where the production yield of monolayer or few-layer sheets could reach as high as 92%.[34] Moreover, the exfoliation by the electrochemical process can be achieved at room temperature within several hours, significantly improving the production efficiency.

Compared with the mechanical exfoliation, the yield of 2D materials by chemical exfoliation is significantly improved. However, the disadvantages of the chemical methods are obvious. The products degraded due to the change of the lattice structure,[33] Hence, it is necessary to perform post-treatment to reconstruct the layer structure.[36] Also, because the sonication is required, the 2D materials sheets obtained are non-uniform small in lateral dimension,[37] which makes the large-scale device fabrication challenging.

Vapor phase deposition. Vapor phase deposition is a technique to prepare atomically thin flakes or films by directly depositing desired vapor-phased compounds with or without chemical reaction to form layers on specified substrates. By this technique, 2D material preparation can be realized with good crystallinity, high layer controllability, and large-area uniformity. Generally, vapor phase deposition includes three main approaches: metal transformation by sulfurization or selenization, thermal decomposition of precursors, physical vapor deposition (PVD), and chemical vapor deposition (CVD).

Metal transformation is an easy way to prepare atomically thin films. Zhan et al.[38] prepared MoS_2 film by depositing Mo thin film on SiO_2 substrate first, followed by sulfurization to transfer Mo to MoS_2 (Fig. 2a–c). They successfully obtained single layer to few-layered MoS_2 films by this method. Also taking the thermal decomposition of thiosalts for MoS_2 preparation as the example, the MoS_2 thin layers were prepared by the two-step thermolysis process of ammonium thiomolybdate (Fig. 2d).[39] Firstly the $(NH_4)_2MoS_4$ thin film was prepared by dip-coating in $(NH_4)_2MoS_4$/dimethylformamide (DMF) solution followed by annealing process to remove the residual solvents, NH_3 and other by-products dissociated from the precursors. Then $(NH_4)_2MoS_4$ conversed to MoS_2 during the second annealing process with higher temperature in the presence of sulfur vapors, which helped remove the defects caused by oxygen species and improve the crystallinity of MoS_2 thin layers. The limitation of metal transformation and thermal decomposition of precursors is the insufficient controllability of the thickness and uniformity of the pre-prepared films (such as the deposited Mo film or the $(NH_4)_2MoS_4$ thin film), as well as the polycrystalline nature of the as-synthesized film, making its application restricted.

PVD approach is to obtain 2D materials by recrystallization of materials through a vapor-solid process. Various 2D materials can be prepared by PVD process. Taking In_2Se_3 as an example, Lin et al.[40] first reported the synthesis of atomically thin In_2Se_3 flakes with this method. By using In_2Se_3 powders as the precursor and graphene (or mica) as the substrates, orientation-defined In_2Se_3 flakes with the thickness less than 3 layers could be achieved under the negative pressure (50 Torr). By controlling the cooling rate during the growth process, the crystalline phases of as-obtained In_2Se_3 could be adjusted. Zhou J. et al.[41] later reported the preparation of the high-quality monolayer α-In_2Se_3 material by PVD method under atmospheric pressure and observed the Raman and PL signals in monolayer In_2Se_3 for the first time (Fig. 2e–i). However, the random nucleation of the crystals in PVD can make the layer thickness uneven, which requires more research

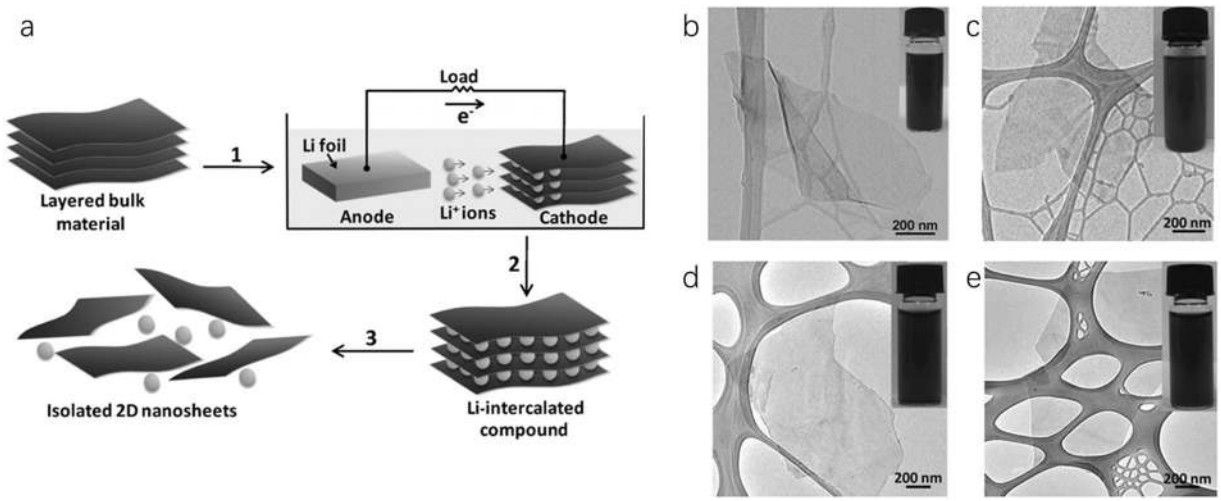

Fig. 1 Electrochemical lithiation process for the fabrication of layered 2D nanosheets from bulk material. **a** Schematic illustration of electrochemical lithiation process. **b**–**e** TEM images of typical 2D nanosheets got by electrochemical lithiation process. Inset: Photographs of the corresponding solution. **b** MoS_2, **c** WS_2, **d** TiS_2, **e** TaS_2 (reproduced with permission from ref.[34], Copyright John Wiley and Sons, 2011)

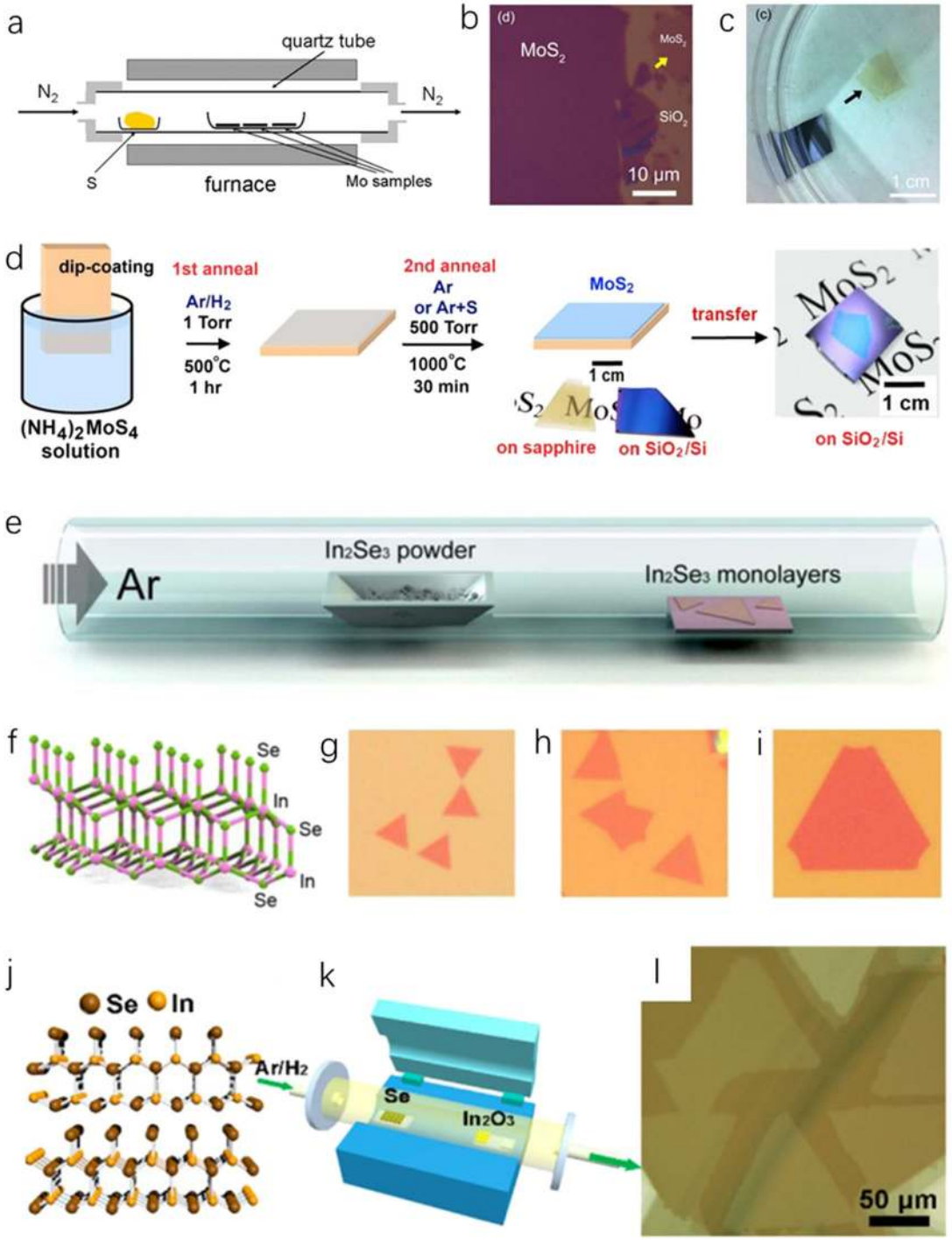

Fig. 2 Vapor Phase Deposition Growth of 2D materials. **a**–**c** synthesis of MoS_2 by selenization of Mo thin film. **a** Schematic illustration of metal transformation for MoS_2 film preparation. **b** Optical image of MoS_2 on SiO_2/Si substrate. **c** SiO_2/Si substrate (left) and peeled off few layer MoS_2 (right) (reproduced with permission from ref.[38], Copyright John Wiley and Sons, 2012). **d** Schematic illustration of the thermal decomposition of $(NH_4)_2MoS_4$ for the synthesis of MoS_2 thin layers on insulating substrates (reproduced with permission from ref.[39], Copyright American Chemical Society, 2012). **e**–**i** Synthesis of 2D In_2Se_3 flakes by PVD method. **e** Schematic illustration of PVD process for In_2Se_3 layers with In_2Se_3 powders as precursors. **f** Crystal structure of In_2Se_3 monolayer. **g**–**i** Optical images of In_2Se_3 with the growth time of 5, 10, and 15 min, respectively. The scale bar is 5, 10, and 10 μm, respectively (reproduced with permission from ref.[41], Copyright American Chemical Society, 2015). **j**–**l** Synthesis of 2D In_2Se_3 flakes by CVD method. **j** Crystal structure of α-In_2Se_3. **k** Schematic illustration of the CVD growth process of 2D In_2Se_3 on mica substrates. **l** Optical microscope image of as-grown triangular In_2Se_3 nanosheets on mica substrate (reproduced with permission from ref.[42], Copyright American Chemical Society, 2016)

efforts to resolve the issue.

CVD is a kind of technique to produce thin films on substrates through the chemical reaction of volatile precursors. 2D materials produced by CVD method have shown very-high quality with a scalable size and controllable thickness, making it promising for the application in electronic industry. According to Feng et al.[42] mono-, bi-, and trilayer α-In_2Se_3 flakes could be synthesized on mica substrates by CVD method using Se and In_2O_3 powders as the precursors in the H_2/Ar atmosphere, and the as-synthesized In_2Se_3 flakes could be as large as 100 μm lateral dimensions (Fig. 2j–l). Yu et al.[43] used metal organic chemical vapor deposition (MOCVD) to prepare polycrystalline In_2Se_3 film. They used trimethylindium and ditertiarybutylselenide organic compounds as the precursors and Ar as the carrier gas, and the process was carried under the pressure of 10–80 torr. By CVD techniques, it not only can produce 2D material with good quality, high yield and large lateral size, but also offer a way to construct heterostructure with a clean interface, which is desirable for both fundamental research and device applications.

The characterization methods of piezoelectricity/ferroelectricity

With the dimension reducing towards nanometers, macroscopic characterization methods for piezo/ferroelectricity, such as the "Sawyer-Towler-circuit" method based on charge testing or "Virtual-ground" method based on current testing, are not suitable anymore for characterization of small size 2D piezo/ferroelectric anymore. New alternative methods for the nanoscale characterization have thus been developed. In this section we will review these emerged characterization technologies. By combining these different advanced tools, it is possible to investigate the piezoelectricity/ferroelectricity towards atomic layer thickness from different aspects, advancing our understanding of piezo/ferroelectric mechanism in nanoscale, and finally provide insights into the new material design and device innovation.

Piezoelectric force microscopy. Piezoelectricity is a property of a material that generates electric potential upon an applied mechanical stress, whereas inverse-piezoelectricity is a property of a material that generates mechanical deformations upon an electric field. The basic principle of (Piezoelectric force microscopy) PFM is using the inverse-piezoelectric effect: an ac field is applied onto the sample surface through the AFM probe, which results in the surface deformation (vertical expansion/retraction and lateral torsion) of the sample.[44] The amplitude/phase of this subtle deformation could be used to characterize the strength/direction of the dipole. PFM has been widely used to characterize the piezoelectric and ferroelectric materials, such as quantitative determination of piezoelectric coefficient,[45] the ferroelectric domain imaging and domain switching dynamic behaviors.[46] Specifically, a combined local butterfly-like amplitude switching loop and 180° phase reversal loop under the external electric bias, together with the switched domains induced by the opposite voltages are usually utilized to confirm the ferroelectric properties of the material. However, many non-ferroelectric materials could also show similar behaviors due to the coulombic electrostatic interaction between the AFM tip/cantilever and the charged sample surface, or the electrical driven ion accumulation/depletion induced sample deformation.[47,48] These effects can be largely avoided by producing a homogeneous electric field through a top metal electrode, by advanced voltage pulse protocol, and through combined characterization with other tools such as Kelvin probe force microscopy.[44] Many excellent reviews have been published over the years on the PFM characterization,[44,48–51] and the reader is referred to these reviews for further information.

Second-harmonic generation method. SHG is a nonlinear optical process in which two incident photons of the same frequency ω, when interacting with a material, could generates an output photon of twice the frequency 2ω. This frequency-doubling process can only occur in materials that lack inversion symmetry, making SHG a sensitive probing tool for the characterization of piezoelectric and ferroelectric materials. Specifically, SHG has been widely used for the investigation of piezoelectric,[9,45] paraelectric-ferroelectric transition,[13,52] and the ferroelectric domain imaging and switching.[53] Denev S. A. et al. has given an excellent review on the ferroelectric probing by SHG,[54] and the readers are referred to this review for more information. Generally both PFM and SHG technologies are non-destructive, making them very useful for thin film characterizations, where traditional electric measurements based on capacitor-charging fails due to the weak polarization and the strong electric leakage of thin film. Recently, SHG has been used to determine the Curie temperature of 2D ferroelectric CIPS flakes down to 4 nm thickness.[13] Compared with PFM, SHG have proven to be extremely sensitive to the changes of structure symmetry, which allows for the detection of ferroelectric-paraelectric phase transition and the determination of Curie temperature, while PFM can have a very-high spatial resolution (~several tens nm dependent on the tip radius) compared with that of SHG (~hundreds nm depends on the incident light wavelength), which is beneficial for high-resolution domain imaging.

Other characterization methods. According to the definition, piezoelectric/ferroelectric occurs in materials lack of inversion symmetry, so generally structure characterization tools such as synchrotron X-ray scattering, scanning transmission electron microscopy (STEM), scanning tunneling microscopy (STM), and ultraviolet Raman spectroscopy (UV-Raman) can be utilized for piezo-/ferro-electric characterizations. Chang K. et al. has proved the robust ferroelectricity of SnTe in a single unit cell thickness (~0.63 nm) by using STM (see section 4 for more details).[11] Tenne D. A. et al. has found that single unit BTO (~0.4 nm) in BTO/STO superlattices is ferroelectric up to 250 K by using UV-Raman.[55] Fong D. D. et al. confirmed the ferroelectricity and observed the 180° vertical domain structure of 1.2 nm ultrathin PZT film at room temperature by using synchrotron X-ray.[56] And recently, Gao. P et al obtained a residual polarization as high as ~16 μC/cm^2 for 0.6 nm PZT film by using quantitative annular bright field imaging mode in STEM.[57]

PIEZOELECTRIC 2D MATERIALS

Piezoelectricity refers to the ability of a non-centrosymmetric material to generate polarization charges in response to the externally applied mechanical stress. Since its discovery in 1880, plenty of materials, including crystals, polymer, and bi-molecules, have been reported to possess the piezoelectric responses. Moreover, many of these piezoelectric materials have found extensive applications in actuators, sensors, and energy harvesting systems.[58–60] Basically, the piezoelectric coupling of mechanical and electrical behaviors for a crystal can be depicted as $S_{ij} = d_{kij}E_k\ (i,j,k = 1,2,3)$, where S, d, and E donate the second-rank strain tensor, piezoelectric coefficient and the electric field, respectively; i, j, and k represent x, y, and z of the Cartesian reference frame.[61] The orientation of the applied strain tensor (compressed strain or tensile strain) can consequently switch the piezoelectric polarization (electric field) direction. Additionally, the converse piezoelectric effect has also been widely used for production of sound waves and in AFM systems.

Besides, the demands for small-scale and diverse-functional devices are particularly urgent. In these regards, 2D piezoelectric nanomaterials become exceedingly intriguing due to their ultrathin geometry, excellent electromechanical response, and other unique physical properties.[9,62] Furthermore, they are expected as the promising candidates and platforms for

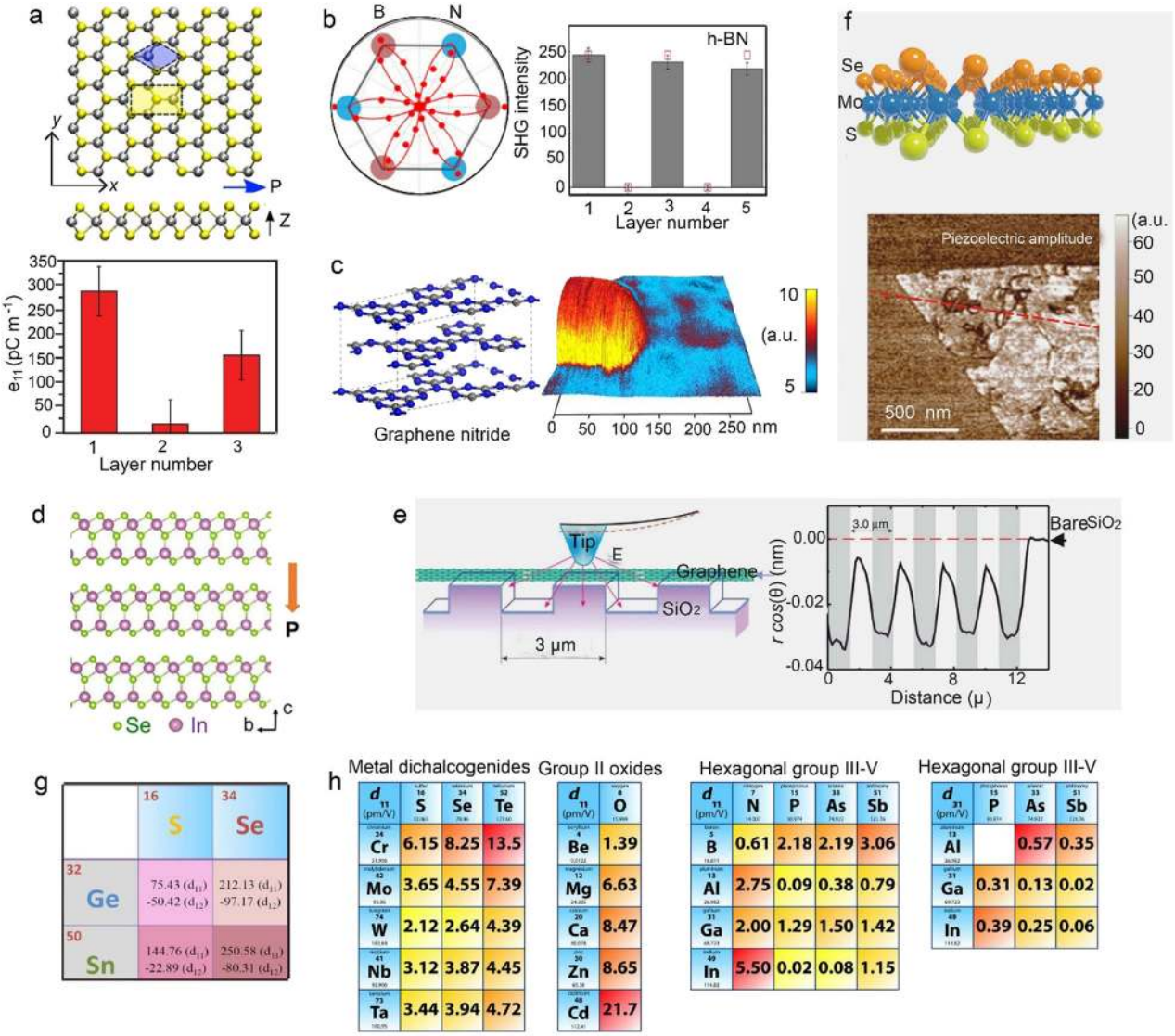

Fig. 3 Piezoelectricity in various 2D materials. **a** Top view and side-view geometries of trigonal prismatic molybdenum disulfide monolayer (2H-MoS_2). Measured piezoelectric coefficient in one-, two-, and three-layer MoS_2 are shown at the bottom panel (reproduced with permission from ref.[10], Copyright American Chemical Society, 2012, and ref.[45], Copyright Springer Nature, 2014, respectively). **b** The layer dependence of SH intensity for layered h-BN (adapted with permission from ref.[68], Copyright Springer Nature, 2013). **c** Layered tri-s-triazine (graphene nitride: g-C_3N_4) sheets and corrected vertical PFM amplitudes (reproduced with permission from ref.[69], Copyright Springer Nature, 2014). **d** Side-view crystal structure of α-In_2Se_3 in the space group of R3m. The piezoelectric polarization direction is labeled as the arrow shows (adapted with permission from ref.[71], Copyright American Chemical Society, 2017). **e** Schematic of the PFM measurements on single-layer graphene adsorbed on the TGZ4 grating substrates and cross-section of the piezoresponse along the line on graphene across the grating structures (shaded areas corresponding to supported graphene) (adapted with permission from ref.[72], Copyright Springer Nature, 2015). **f** Piezoelectric amplitude of an isolated Janus MoSSe monolayer directly grown on HOPG, measured by resonance-enhanced piezoresponse force microscopy (adapted with permission from ref.[74], Copyright Springer Nature, 2017). **g** Predicted piezoelectric properties of group IV monochalcogenides (adapted with permission from ref.[18], Copyright AIP Publishing LLC, 2015). **h** Periodic trends for d_{11} in metal dichalcogenides, metal oxides, and group III–V semiconductors as well as for d_{31} in group III–V semiconductors (reproduced with permission from ref.[21], Copyright American Chemical Society, 2015)

innovative design and development of future nanomechanical system, self-adaptive nanoelectronics/optoelectronics, and smart robotics.

In-plane piezoelectric materials

We will discuss the experimentally confirmed in-plane piezoelectric materials: TMDC, h-BN, and graphene nitride. The first group introduced here is the family of hexagonal transition metal dichalcogenide (h-TMDC). Each individual layer of TMDC is constructed by a metal plane sandwiched between two dichalcogenide planes, whose basic unite cell adapts to the trigonal prismatic structure with metal atoms residing at the center.[63] For piezoelectric materials, non-centrosymmetry analysis is a direct and effective method to estimate the existence of piezoelectricity.[61] Here, we take monolayer MoS_2 as an example for its analogous TMDC to interpret the origin of the piezoelectricity as shown in Fig. 3a. In 2012, based on DFT calculation, Reed et al first predicted that monolayer TMDC materials are piezoelectric, unlike their bulk crystals.[10] Two year later, Wu et al demonstrated this prediction using the flexible MoS_2 piezoelectric nanogenerator (see Fig. 4a for more details).[9] It can be seen from

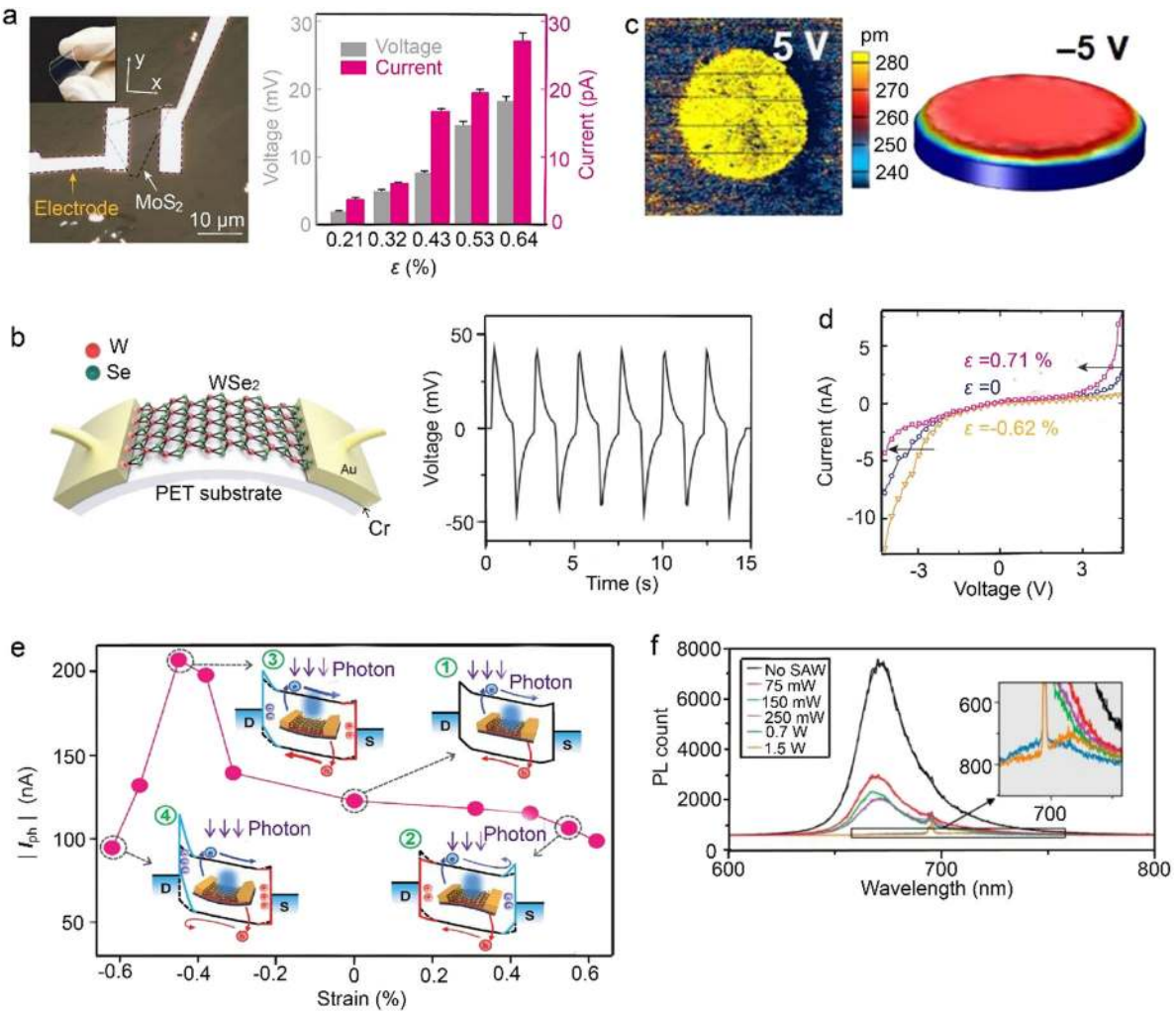

Fig. 4 Applications of 2D piezoelectric materials in energy harvesting, actuators, strain-tuned electronics and optoelectronics. **a** Optical graphs of a flexible monolayer MoS_2 piezo-nanogenerator (left panel) and external strain dependence of the voltage and current outputs (right panel) (reproduced with permission from ref.[9], Copyright Springer Nature, 2014). **b** Schematics of the flexible monolayer WSe_2 piezoelectric nanogenerator and its piezoelectric voltage responses (adapted with permission from ref.[65], Copyright John Wiley and Sons, 2017). **c** Vertical PFM amplitude image for CdS thin film with the drive voltage of 5 V and the simulation of subatom deformation actuators in the presence of −5 V voltage bias (adapted with permission from ref.[75], Copyright American Association for the Advancement of Science, 2016). **d** Piezoelectricity of monolayer MoS_2 for the asymmetry modulation of the carrier transport in the electrical device as shown in (**a**) (reproduced with permission from ref.[9], Copyright Springer Nature, 2014). **e** Photocurrent as a function of the applied strain for the single-layer MoS_2 flexible device and the correlated working mechanism (reproduced with permission from ref.[82], Copyright John Wiley and Sons, 2017). **f** The PL emission is tuned by the SAW induced piezoelectricity in monolayer MoS_2. SAW represents surface acoustic wave, that is used to produce strain in monolayer MoS_2 (reproduced with permission from ref.[83], Copyright American Chemical Society, 2016)

the top view structure (the top panel of Fig. 3a) that the monolayer MoS_2 does not have an inversion center. This non-centrosymmetric structure provides the direct evidence of the piezoelectric effect for the monolayer MoS_2. Note that this piezoelectric property only restricts to the in-plane (d_{11}) direction and doesn't involve to the out-of-plane (d_{33}) direction because monolayer MoS_2 retains the ideal symmetry feature along the vertical *z*-axis as shown in the middle panel of Fig. 3a. While suffering an external strain, monolayer MoS_2 inherently generates electric dipoles resulting from the displacement of cation Mo and anion S atoms. These inner electric dipoles give rise to the emergence of piezoelectric polarization charges at the material surfaces and the related piezoelectric field across the entire material. Moreover, because of the unique hexagonal structure of monolayer MoS_2, the in-plane piezoelectric field vector owns three equivalent directions that are along the semiconductor's three-fold symmetry axis. As verified by the reported SHG signals and piezoelectric coupling strength,[9,45] the asymmetry and piezoelectric responses exhibits strong angle dependence and the corresponding maximum occurs at a multiple of 60° (defining the "armchair" direction as 0°). Interestingly, bilayer MoS_2 gives the same planar atom projections at the six vertex sites of hexagonal structure and thus keeps the crystal centrosymmetry, resulting in the loss of piezoelectric effect.

In 2014, Zhang et al. have proposed a novel device configuration for detecting the in-plane piezoelectricity in monolayer MoS_2.[45] The suspended free-standing membrane with its two terminals clamped on the metal electrodes can be successfully achieved through several-step nanofabrication technique. The core principle for this measurement is to transform the applied voltage induced in-plane strain to the out-of-plane strain by the AFM probe (here AFM tip closely contacts with the membrane). The measured e_{11} piezoelectric coefficient is shown at the bottom panel of Fig. 3a. It's observed that a piezoelectric response only exists in the odd-layer flakes and vanishes in the even-layer flakes. This thickness dependent piezoelectricity in MoS_2 membrane

coincides with the structural non-centrosymmetric analysis above. Inspired by these pioneering works related to MoS_2 piezoelectricity, the studies for piezoelectricity in TMDC have drawn much attention in the research community recently.[64–66]

Layered hexagonal boron nitride (h-BN) is a wide-band insulator and theoretically calculated to possess planar piezoelectric properties in 2009.[67] The boron and nitride atoms in h-BN crystals also arrange in a hexagonal array (the left panel of Fig. 3b). Unlike its counterpart, graphene, monolayer h-BN keeps strong in-plane piezoelectricity due to the alternating arrangement of boron and nitride atoms in the hexagonal vertex site. 1n 2013, Tony F. Heinz et al. utilized optical second-harmonic generation (SHG) to demonstrate the non-centrosymmetric structure of h-BN (the right panel of Fig. 3b),[68] indirectly verifying the existence of h-BN piezoelectricity. Note that along the directions of three-fold symmetry axis, h-BN always exhibits distinct SHG intensity and the SHG signals also show layer dependent effect in virtue of the special crystal structure.

2D graphene nitride, or g-C_3N_4, is the graphitic form of carbon nitride. A single layer of g-C_3N_4 is consisted by the more energetically stable tri-s-triazine arrays. The tri-s-triazine layer of g-C_3N_4 possesses the intrinsically non-centrosymmetric holes in its whole structure, leading to the in-plane piezoelectricity.[69] Unlike TMDC, its multilayer counterpart, even bulk, also possesses strong in-plane piezoelectricity due to the unusual atom-stacking sequence as shown in the left image of Fig. 3c. The PFM amplitude mapping of a g-C_3N_4 particle (~30 nm) is presented at the right side of Fig. 3c and the results confirm the piezoelectricity of multilayer g-C_3N_4.

Theoretically, various 2D semiconductors are predicted to have in-plane piezoelectric effect. The monolayer group IV monochalcogenides (MX, M = Sn or Ge, X = Se or S) are calculated to own peculiar piezoelectricity as shown in Fig. 3g and the d_{11} and d_{12} piezoelectric coefficients are summarized in the table.[18] Remarkably the in-plane piezoelectric coefficient d_{11} for this group semiconductors ranges from 75 pm/V to 250 pm/V, which is almost two orders of magnitude larger than those conventional piezoelectric materials including α-quartz, AlN, GaN, and ZnO. Li et al. predicted that group III monochalcogenides, GaS, GaSe, and InSe, are piezoelectric for the monolayer form, whose piezocoefficient is calculated to be 0.06, 2.30, and 1.46 pm/V, respectively.[70] Using the first-principle calculation, Richard et al. uncovered the existence of in-plane (d_{11}) piezoelectricity in plenty of 2D materials (monolayer form),[21] such as the family of metal dichalcogenides (MX_2, M = Cr, Mo, W, Nb, Ta and X = S, Se, Te), group IIA and IIB metal oxides (MO, M = Be, Mg, Ca, Zn, Cd, Pb), and group III–V materials (AX, A = B, Al, Ca, In and X=N, P, As, Sb) as displayed in Fig. 1h. Their detailed piezoelectric coefficients are also indicated in the image.

Out-of-plane piezoelectric materials

Next, we will turn to the experimentally reported out-of-plane 2D piezoelectric materials. Alpha phase indium selenide (α-In_2Se_3), as a typical III–VI semiconductor, is reported to be a stable and layered structure among the five phases at various temperatures. Multilayer rhombohedral α-In_2Se_3 has been demonstrated to exhibit out-of-plane piezoelectricity based on the TEM and SHG structure analysis.[71] The detailed crystal structure is schematically displayed in Fig. 3d. We can see that one quintuple layer consists of five adjacent atom layers (Se-In-Se-In-Se) and the corresponding structure presents the asymmetry property. Under external strain, the produced electric dipole pointing from negative selenide atom to positive indium atom can result in the vertical (out-of-plane) piezoelectric field as the arrow shows. Of course, when thinning down the thickness to several nanometers, many conventional buckled hexagonal materials, such as CdS membrane and ZnO nanofilm, still preserve the out-of-plane piezoelectricity like the bulk counterparts.

Structural nonocentrosymmetry is a well-known origin of the intrinsic piezoelectricity while some special interfaces can also give rise to the formation of out-of-plane polarized dipoles, which can be called “extrinsic piezoelectricity”. Note that the piezoelectricity for all the mentioned materials in this review is intrinsic unless otherwise specified, like this paragraph. One case is the doping effect between graphene and the supported substrate Graphene is known as a perfect and centrosymmetric hexagonal material with one type of carbon atoms and don’t have piezoelectric effect. However, since the supported substrate, such as silica, often introduces some chemical substances into graphene, namely doped graphene, its symmetry structure will be unintentionally broken, resulting in the generation of out-of-plane dipole (piezoelectricity) as indicated in Fig. 3e.[72] The PFM response on bare SiO_2 is also shown to be a crucial reference for the PFM amplitude observed on graphene, clearly clarifying that the piezoelectric response comes from the graphene deposited on silica substrate. Here the interfacing chemical interaction between the carbon atoms in graphene and oxygen atoms in silica can generate non-zero electric dipole moment and polarization, leading to the piezoelectricity of the supported graphene. The other case is the ferroelectric-substrate induced extrinsic piezoelectricity in multilayer MoS_2 lying on $PbTiO_3$ film.[73] This out-of-plane dipole effect in MoS_2 flakes, trigged by ferroelectric polarization, is more pronounced for the 19 nm specimen.

Theoretically, apart from the in-plane piezoelectricity, the monolayer buckled hexagonal materials are estimated to have out-of-plane piezoelectric effect as well.[21] These materials includes most of group III–V materials (AX, A = Al, Ca, In and X = P, As, Sb; but except for AlP) as shown in Fig. 3h.

In-plane and out-of-plane intercorrelated piezoelectric materials

In addition, some special material can exhibit intricate piezoelectricity by the coupling of in-plane and out-of-plane piezoelectricity. Recently, Janus MoSSe monolayer with broken out-of-plane symmetry is innovatively synthesized by the plasma stripping and thermal selenization.[74] In this structure, one S-atom layer in monolayer MoS_2 is artificially replaced by the Se-atom layer as shown in Fig. 3f, exhibiting the out-of-plane piezoelectricity that will not appear for the pristine monolayer MoS_2. PFM signal has been used to characterize the vertical piezoelectricity as shown in the bottom panel of Fig. 3f. Moreover, such Janus monolayer should also possess the in-plane piezoelectric effect owing to the similar atom planar projections with TMDC family. Interestingly, CVD synthesized rhombohedral α-In_2Se_3 flakes have been demonstrated as in-plane and out-of-plane ferroelectric, from which we can scientifically infer that this material should also keep the in-plane and out-of-plane piezoelectricity (because a ferroelectric material must possess the piezoelectric effect).

We have summarized the piezoelectric properties as shown in Table 1 for the experimentally confirmed typical piezoelectric 2D materials. Generally, the feature of non-centrosymmetry is the sufficient requirement for piezoelectric materials (except for the cubic class 432). By symmetry analysis, one can preliminarily conclude whether a 2D material is piezoelectric or not.[61] Although various 2D materials have been theoretically predicted to be piezoelectric, most of them need to be further explored or confirmed by experiments.

Applications of 2D piezoelectric materials

With the fundamental study of piezoelectricity in 2D materials, a series of correlated interesting applications successively emerge in the field of energy harvesting, actuators, strain-tuned electronics, and optoelectronics. In this section, we will systematically review

Table 1. Summary of the experimentally confirmed piezoelectric 2D materials

2D materials	Crystal structure	Piezoelectric direction	Estimated piezocoefficient	Notes
Monolayer MoS_2	Hexagonal	In-plane Angle dependence	$d_{11} = 2.5 - 4$ pm/V[10] $e_{11} = 250 - 400$ pC/m[10,45]	Odd-even effect with the thickness increased
Monolayer h-BN	Hexagonal	In-plane Angle dependence	$e_{11} = 100 - 400$ pC/m[10]	Odd-even effect with the thickness increased[68]
Graphitic carbon nitride		In-plane	$e_{11} = 218$ pC/m[69]	Existence of piezoelectricity regardless of thickness
Doped graphene	Hexagonal	Out-of-plane	$d_{33} = 1.4$ nm/V[72]	Extrinsic piezoelectricity
α-In_2Se_3	Rhombohedral	Out-of-plane & in-plane		Indirectly confirmed by the ferroelectricity[17]
Janus MoSSe	Hexagonal	Out-of-plane & in-plane	$d_{33} = 0.1$ pm/V[74]	

the latest progress on the application of 2D piezoelectric materials.

Energy harvesting. The energy harvesting cells based on 2D piezoelectric materials are crucial for future wireless nanosystems without power supply, such as environmental monitors, implantable medical sensors, and personal electronics. In 2014, Wu et al. pioneered a monolayer MoS_2 as prototype nanogenerator for scavenging the mechanical energy.[9] Optical image of a typical nanogenerator is shown in the left image of Fig. 4a. As for this nanogenerator, it will generate a peak voltage or current signal only during the moment of stretching and releasing. With the increasing tensile strain, both the peak voltage and current increase. Furthermore, this type of device can still maintain a stable output even after three hours of fatigue test, demonstrating its excellent performance for harvesting various tiny mechanical vibration energies. Enlightened by this work, Lee et al. developed a monolayer WSe_2 piezoelectric nanogenerator, which gives a peak voltage of 45 mV under a strain of 0.39 % as shown in Fig. 4b.[65] In this work, to enhance the piezoelectric outputs, CVD synthesized monolayer WSe_2 samples have been successfully transferred to the top of another one to form a special-orientated artificial bilayer (AA stacking), which could retain the piezoelectric effect, unlike its natural or pristine form. The piezoelectric coefficient for artificial bilayer can be about two times larger than that of the monolayer flakes.

Actuators. An actuator is often used to produce a mechanical motion for moving or controlling a system, which acts as an important role in modern life. Utilizing the reverse piezoelectric effect, piezo-ceramics have been extensively employed to produce mechanical vibrations with an applied bias voltage. For the 2D prototypical piezo-actuators, it can be exemplified in the ultrathin piezoelectric CdS film as shown in Fig. 4c,[75] where the left image shows the vertical (out-of-plane) piezo-responses probed with PFM amplitude image. Through simulation by COMSOL, the CdS thin film driven by a negative voltage of −5 V, can generate an expansion of 150 pm, which is sufficient to achieve accuracy displacement or control for some mechanical systems.

Strain-tuned electronics and optoelectronics. Piezoelectric polarization charges induced at the surfaces of 2D materials can be used to modulate the conductivity of the as-fabricated devices via Schottky barriers, which is extremely vital for future robotics, wearable electronics, and human-interfacing.

Piezotronic devices, a new and useful prototype, are to exploit piezoelectric polarized charges to serve as 'gate' for modulating the carrier transport of the device,[76–78] that is a fundamentally different operation process from the electrically gated electronics. The first 2D materials based piezotronic devices is successfully implemented in PET supported MoS_2 flakes[9] as indicated in Fig. 4d. The asymmetry change in the output curve shall be attributed to the piezotronic effect which modulates the metal-MoS_2 contacts.

Piezophototronic devices are based on the piezo-polarized charges to tune/control the inner carrier generation, separation, diffusion, and recombination.[79–81] The design for this novel device has been also demonstrated in the monolayer MoS_2 photodetectors[82], as shown in Fig. 4e. It's observed that strain triggered polarization charges can evidently modulate the separation of photo-carriers. Applying a feasible strain on the photodetector allows one to obtain enhanced or quenched photocurrent. In addition, the inherent piezoelectricity in monolayer MoS_2 is reported to reversibly tune its dynamic recombination of photon excited excitons or trions.[83] The external strain is introduced by the surface acoustic wave (SAW). With the increase of SAW power, the intensity of PL emission will drastically decrease as shown in Fig. 4f, which is associated with the piezoelectricity induced spatial separation of more electrons-holes quasi-particles.

FERROELECTRIC 2D MATERIALS

Ferroelectric materials is a subset of materials that possess spontaneous polarization states in the absence of an electric field, and the application of a large enough electric field can induce the polarization switching between these states. Typically, ferroelectric materials only display these features below the Curie temperature (T_c), where a structure transition from high-symmetry to low-symmetry occurs. Different from piezoelectric, which describes a subset of materials that could possess electric polarization only upon the applied external stimulus-stress, ferroelectric materials possess remanent polarization even after removing the external stimulus-electric field. All ferroelectric materials have piezoelectric and inverse-piezoelectric properties, which make them being used as stress sensors, actuators, and energy converters as discussed in the last section. While using the remanent polarizations states and their feasible switching behavior under external electric field, ferroelectric materials can be used as non-volatile random access memories, which have attracted considerable interest nowadays and will be covered in this section. Continuing quests for higher storage density, low power consumption, and stronger sensitivity drive various explorations of ferroelectrics towards reduced dimensions. Due to the cooperative behaviors of electric dipoles[56,84,85] and the depolarization effects correlated with uncompensated interfacial charges,[86–88] ferroelectric films were expected to keep a stable polarization only above a critical thickness of around tens of nanometers. With the development of thin film fabrication, especially the advancement in perovskite oxides, it is now believed that ferroelectricity could retain down to several unit cells for traditional perovskite oxide, such as $PbTiO_3$ down to 1.2 nm,[56] $BaTiO_3$ down to 2.4 nm,[89] and $BiFeO_3$ down to 3 nm.[90] Ferroelectricity could even be enhanced at low dimensions through some special mechanism as shown in ultrathin strain free $SrTiO_3$ films.[91] However, retaining the functional properties of

ferroelectric oxides at the reduced dimensions usually requires a careful selection of oxide substrates with small lattice mismatch to that of ferroelectrics, largely limiting their potential applications in modern nanoelectronics. In addition, various defects such as oxygen vacancies is inevitable during high temperature thin film growth and nanostructure fabrication, which could deteriorate the intrinsic ferroelectric properties.[92] Recently, lots of attention has also been devoted to simple binary oxides of HfO_2 and ZrO_2,[93,94] which show robust ferroelectricity/antiferroelectricity upon element doping like Si, Al, Y, Ga, La, and Sr.[95] Ferroelectricity has been found in $Hf_{0.5}Zr_{0.5}O_2$ down to a thickness of ~2.5 nm.[96] There has been some excellent reviews and book chapters discussing the development of this non-traditional ferroelectrics.[97,98] Compared with the traditional ferroelectric oxides and HfO_2/ZrO_2 system, 2D materials is free of dangling bonds, offering merits like high carrier mobility,[99] band gap tunablity,[100] and structure flexibility.[9] More importantly, they could be integrated into van der Waals heterostructures flawlessly. Studying 2D ferroelectrics is thus highly technological important. The first 2D ferroelectricity has been reported two decades ago in PVDF organic polymers,[16] which however does not draw enough attention. The pioneer work on graphene[1] in 2004 has triggered the intensive research on 2D materials and provoked the searching of 2D ferroelectrics. Many 2D ferroelectric materials were theoretically predicted, including the in-plane ferroelectrics, such as group IV monochalcogenides MX (M = Ge, Sn; X = S, Se)[15]; the out-of-plane ferroelectrics including 1T MoS_2,[101] GaAs[102], and P_2O_3[103]; and finally the intercalated ferroelectrics, such as III_2–VI_3 compounds (A_2B_3 with A = Al, Ga, In, B = S, Se, Te).[14] But to date, experimental reports of 2D ferroelectric remain scare. Here we will review the recent development of this emerging field, including physical properties of various types of 2D ferroelectric materials and their potential applications.

Typical ferroelectric 2D materials

In-plane dominated ferroelectricity. It was believed that ferroelectricity can only sustained down to a critical size of several tens of nanometers due to the depolarization effect.[86–88] Benefit from the improvement in thin film fabrication process and the characterization technology, ferroelectricity has been observed in ultrathin oxide thin films of several nanometers.[55,56] It is realized that many other factors such as the chemical bonding, the interface charge screening effect, and interfacial misfit strains can stabilize the ferroelectric polarizations at the nanometer scale.[56,91,104] Recently, by using the high-resolution STM, Chang K. et al. have put forward this ferroelectric limit towards 1 unit cell.[11] They observed a robust spontaneous polarization in 1-uc thick SnTe film. As shown in Fig. 5a, bulk SnTe possesses a rock-salt structure at room temperature which undergoes a cubic-to-rhombohedral structural phase transition with the two sublattices of Sn and Te atoms displaced from each other along the [111] direction and forming the ferroelectric phase below ~98 K.[105] By carefully reducing the concentration of Sn vacancies so the bulk charging screening effect, ferroelectricity has been achieved successfully in SnTe film with curie temperature up to 270 K for 1-uc thickness and above room temperature for 2- to 4-uc films (Fig. 5c). The phenomenon that T_c of SnTe ultrathin film is substantially higher than that of bulk material is unusual, which shall be attributed to several factors including the quantum confinement effect, the band gap opening at the reduced thickness, and the reducing of carrier densities. Similar unusual behavior has been observed before in ultrathin $SrTiO_3$ films due to the electrode confinement effect.[91] Understanding the general physics behind this phenomenon will benefit for exploring new room temperature ferroelectrics. More importantly, the polarization of SnTe lies in the plane of the film and forms stripe domains with a size of ~50 nm (Fig. 5b). This is totally different from the vertical polarization behavior observed in ultrathin oxide films[56,85–91] and the 2D ferroelectric polymer before,[16] where the polarizations are pointing out of the plane and forming 180° domain walls to reduce the depolarization energy. Such an in-plane polarized film could naturally fight against the depolarization fields and in principally could have very-high stability compared with ceramic oxide, promising for memory applications towards the 2D limit.

Out-of-plane dominated ferroelectricity. CIPS is another layered compound exhibiting room temperature ferroelectricity, which contains a sulfur framework with the octahedral voids filled by Cu, In, and P–P triangular patterns (Fig. 5d, e). The spontaneous polarization comes from the off-centering of Cu sublattice and the In sublattice when the temperature is below the T_c. Or strictly speaking, it is a collinear two-sublattice ferroelectric with Cu and In sublattice rotating simultaneously under an external electric field. Different from SnTe, bulk CIPS holds out-of-plane polarizations[12] with a curie temperature of ~315 K. Interestingly, such an OOP polarization survives towards the 2D limit of ~1.6 nm as recently confirmed by Liu et al.,[13] where PFM has been utilized to characterize ferroelectricity for the ultrathin films. PFM uses the inverse-piezoelectric effect to characterize ferroelectricity, with PFM amplitude reflecting the magnitude of the polarization and the PFM phase indicating the polarization direction.[44,106] As shown in Fig. 5f, g, obvious phase contrasts only exist in the OOP direction whereas there is no phase contrast in the layer plane (Fig. 5h, i), confirming the OOP polarization of CIPS down to 2 L ~ 1.6-nm thickness. One of the interesting observations is that, there is a robust domain evolution in CIPS: the domain pattern changes from dendrite-like pattern into fractal one when the thickness decreases, which is totally different with the IP stripe pattern of SnTe.[11] The origin of these vast different domain patterns is still unclear and worthy of further study. Another interesting observation is the constant T_c independent on the film thickness as shown in Fig. 5j, where SHG signal shows the same upward trend with lowering the temperatures, for film thickness varying from 100 to 10 nm. This is different from that of the oxide ferroelectrics where T_c usually decreases with a reduced thickness.[56,85–88] This abnormal behavior may stem from the fact that CIPS is a layered ferroelectric with very weak interface bonding to the substrate and so T_c is more generally an intrinsic property, whereas the three-dimensional nature of other oxide ferroelectrics usually requires the matching substrate with a correct lattice constant and thus the T_c more relies on the interface bonding. Another factor is the anti-alignment dipole in CIPS which could largely reduce the depolarization field inside the CIPS; thus, this helps to stabilize the polarization down to ultrathin thickness. From this point of view, CIPS is more precisely a collinear ferrielectric rather than a ferroelectric, which however have two Cu sublattices reorient simultaneously under the external electric field.[12] There are very few ferrielectrics with a relative large room temperature polarization (>0.1 μC/cm^2),[12,107] let along the 2D ferrielectric, and obviously more research efforts are needed in the future.

In addition to the robust domain patterns, manipulation of polarization between opposite polarization directions by external electric fields is another typical character of ferroelectricity. This can be easily realized in PFM by applying a vertical electric field between the probe and the sample surface and detecting the surface deformation simultaneously. As shown in Fig. 6k, clear switching of local phase hysteresis loop and butterfly-like amplitude loop unambiguously demonstrate the ferroelectricity of CIPS down to 4 nm thickness.

Intercorrelated ferroelectricity. In addition to the above mentioned 2D ferroelectric with single polarization component (either OOP or IP), there is a third type of 2D ferroelectric that possesses both OOP and IP polarizations. This theoretical prediction was first proposed by Ding W. J. et al.[14] for α-In_2Se_3. By using first-principle

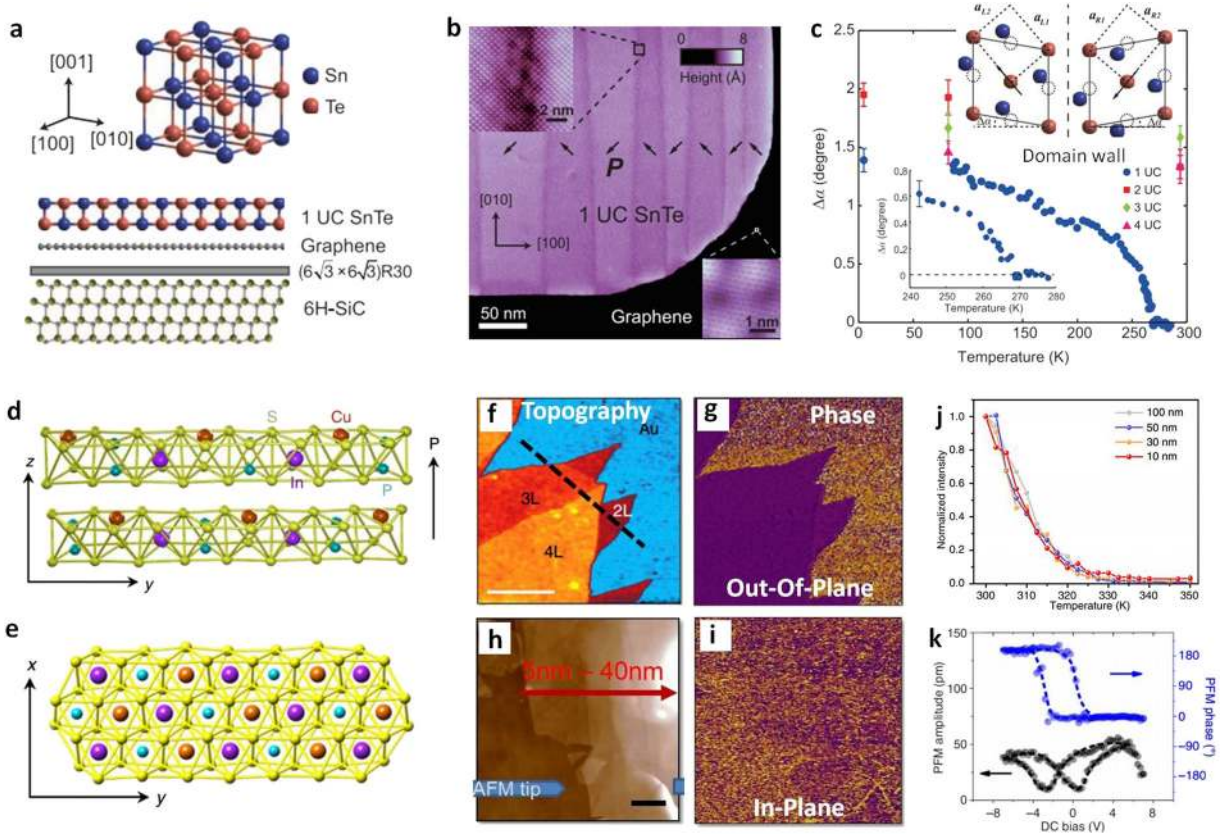

Fig. 5 2D ferroelectric with single polarization component. Top panel, SnTe with IP polarization (adapted with permission from ref.[11], Copyright American Association for the Advancement of Science, 2016). **a** Schematics of the SnTe crystal structure. **b** The stripe domain of a 1-uc SnTe film by STM. The arrows in each domain indicate the direction of lattice distortion. **c** Temperature dependence of the distortion angle for the 1- to 4-uc SnTe films. Inset left, the distortion angle near $T_c = 270$ K for the 1-uc film exhibiting the behavior of a second-order phase transition. Inset right, Schematic of the lattice distortion and atom displacement in the ferroelectric phase. The solid lines indicate the rock-salt unit cell, and the dashed lines indicate the primitive cell of the Te sublattice. The arrows point to the directions of distortion. Bottom panel, CIPS with OOP polarization. **a**–**c** adapted with permission from ref.[11], Copyright American Association for the Advancement of Science, 2016). **d** The side view, and **e** the top view of the crystal structure of CIPS. Within a layer, the Cu, In, and P–P form separate triangular networks. The polarization direction is indicated by the arrow. The OOP piezoresponse images of 2–4 layer thick CIPS flakes with **f** topography and **g** phase. Scale bar in (**f**), 500 nm. The IP piezoresponse images of 5–40-nm thick CIPS flakes with **h** topography, and **i** phase. Scale bar in **(h)**, 1 μm. The substrates are Au coated SiO2/Si. **j** Temperature dependence of the SHG intensity for CIPS flakes with thickness of 100, 50, 30, and 10 nm, respectively. The SHG intensity of each thickness is normalized to its intensity at 300 K. **k** The local PFM amplitude (black) and phase (blue) loops during the switching process of the 4 nm CIPS flake ((**d**–**k**) reproduced from ref.[13])

calculations they show that the α-In_2Se_3 possesses the lowest energy with a variant symmetry breaking Zincblende/Wurtzite crystal structure (Fig. 6a). The lateral movement of Se atoms in the middle layer will lead to the switching of OOP and IP polarizations simultaneously, or say both polarizations are intercorrelated (Fig. 6b). Examining the ferroelectricity of 2D α-In_2Se_3 is a great challenge, partially due to the fact that In_2Se_3 possesses as many as more than five thermodynamic phases.[108] α-In_2Se_3 is the low temperature stable phase, and it is difficult to get highly pure α-In_2Se_3 samples. Details on the fabrication could be seen in the Section one. The other factor is the small atomic shifting between the non-polar and polar Zincblende/Wurtzite structure, which makes the determination of exact crystal structures challenging. The small piezoresponse (~0.05 pm/V)[14] adds another difficulty in examining the 2D ferroelectricity. By using state-of-the-art STEM and resonant PFM on high-quality CVD samples, Cui et al.[17] confirmed not only the crystal structures but also the ferroelectricity of α-In_2Se_3. Figures 6c, d show the OOP and IP box-in-box domains of a 6-nm α-In_2Se_3 flake wrote by the external vertical voltage. Interestingly, the switching of the OOP domains is followed with the IP domains, a direct indication of the intercorrelated polarization behavior of α-In_2Se_3, which originates from the lateral movement of the middle Se layer as shown in Fig. 6b. Such a intercorrelation behavior has been observed in perovskite oxide $BiFeO_3$ before by careful controlling of the interracial strain,[109] now realized the first time in a 2D ferroelectric material.

Another interesting observation is the antiparallel polarization alignment of the interlayer for as-grown α-In_2Se_3 on mica (shown Fig. 6e, f). The IP PFM phase reversed by ~180° depending on the layer thickness, a direct indication of the layer number dependent polarization reversal. Such a behavior has been further confirmed by the local electric field mapping using STEM as shown in Fig. 6g. The direction of the polarization could be quantified through the atomic displacement mapping, which points to [−1010] for 2 L α-In_2Se_3 and reverse to [10-10] for 3 L α-In_2Se_3. A similar odd-even effect of polarization has only been proposed theoretically for few-layer Group IV monochalcogenides MX (M = Ge, Sn; X = S, Se).[15] This experimental observation suggests that the domain walls would tend to appear in the interlayer space for α-In_2Se3, i.e, in the van der Waals gap, different with that of SnTe[11] and CIPS.[13]

Applications of the 2D ferroelectric materials

The remanent polarization due to its non-volatile nature promises the applications of ferroelectricity in storage data memory. 2D

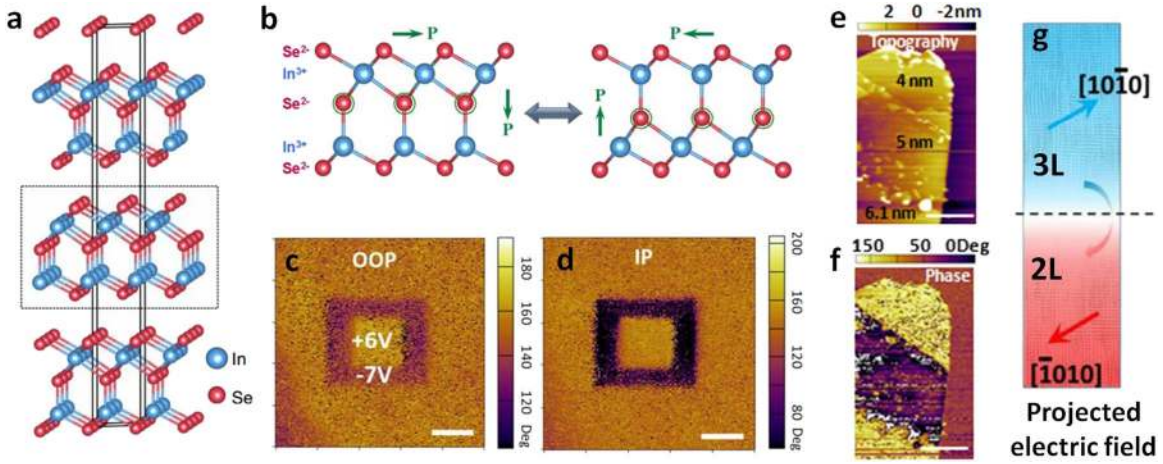

Fig. 6 2D ferroelectric with intercorrelated polarization in α-In_2Se_3. **a** Three-dimensional crystal structure of the layered α-In_2Se_3, with the In atoms in blue and Se atoms in red, and a quintuple layer is indicated by the black dashed square (reproduced from ref.[14]). **b** Schematic model of intercalated IP and OOP switching. OOP (**c**) and IP (**d**) box-in-box phase images wrote by reverse voltage biases of −7 V and +6 V for a 6 nm thick α-In_2Se_3 flake after transferred onto a Au/Si substrate. Scale bar in (**c**) and (**d**), 1 μm. **e** As grown α-In_2Se_3 flakes of different thicknesses on a mica substrate. **f** The corresponding layer dependent IP PFM phase image of the flake. A phase change of ~180° occurs across the interlayer. **g** The projected electric field mapping of an α-In_2Se_3 flake near the 2L-3L boundary using the STEM method. The major direction of electric field in upper and lower regions are close to [10$\bar{1}$0] and [$\bar{1}$010] directions, respectively. **b-g** reproduced with permission from ref.[17], Copyright American Chemical Society, 2018

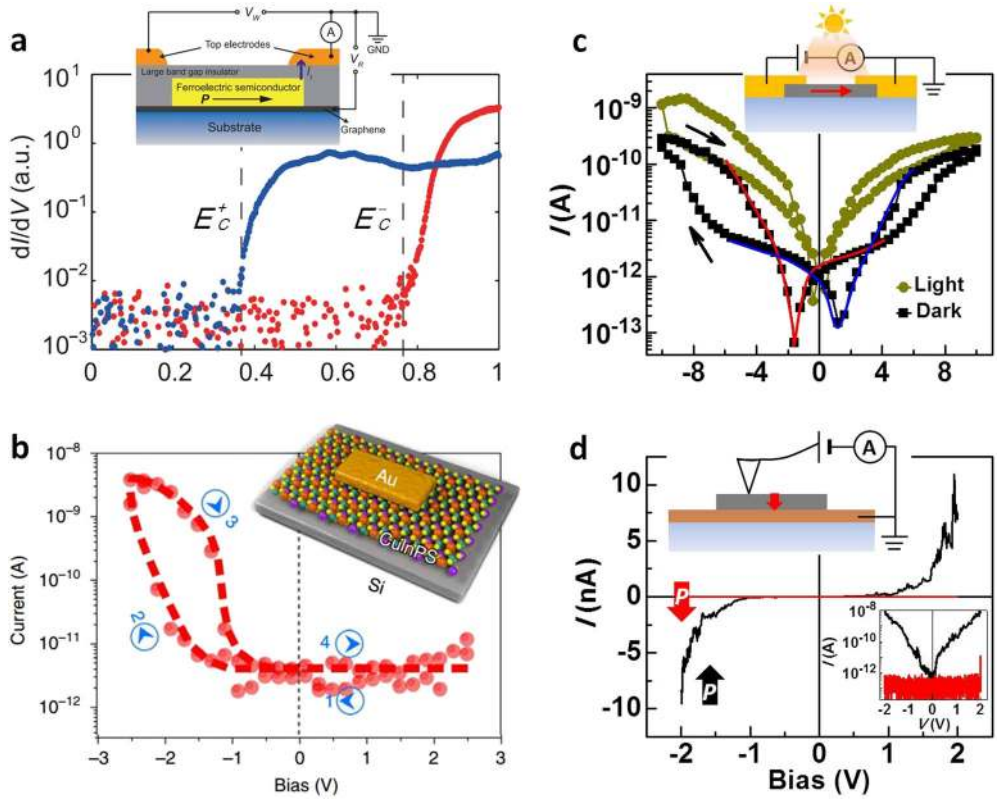

Fig. 7 The prototypical memory devices based on 2D ferroelectrics. **a** SnTe lateral device (adapted with permission from ref.[11], Copyright American Association for the Advancement of Science, 2016). **b** CIPS perpendicular device (reproduced with permission from ref.[13], Copyright Springer Nature, 2016). **c** Lateral and **d** perpendicular devices on the basis of α-In_2Se_3 (adapted with permission from ref.[17], Copyright American Chemical Society, 2018)

ferroelectrics have additional advantages such as the band tuning ability, the miniature size in the OOP direction, and the moderate substrate requirement condition as compared to their ceramic counterparts. These features are beneficial for integrating them as a memory unit in future advanced information technology. Several different non-volatile ferroelectric memory models have been proposed before for traditional perovskite oxide and HfO_2/ZrO_2 thin films, which include (1) the ferroelectric capacitor[110,111] using its charging/discharging function to store information; (2) the switchable diode[112,113] as the result of the polarization modulated

interface barrier; (3) the ferroelectric tunnel junctions[89,114,115] based on the polarization direction dependent tunnel barrier; and (4) the ferroelectric field effect transistor (FeFET) that using the polarization to switch the conduction state (on/off) of the semiconducting channel.[97] These conceptions could be generally extended to 2D ferroelectrics with some specific changes. Based on the polarization direction of 2D ferroelectric as discussed above, several different model memory structures have been proposed. Figure 7a shows the proposed SnTe memory unit which composed of a SnTe film and an insulating cover layer.[11] The voltage between the source and drain is used to modulate the polarization direction and so the band bending on the edge, which will affect the tunneling current between ferroelectric film and the source electrode. Such a three terminal device however is not good for scaling to obtain higher memory density. Whereas for CIPS[13] and α-In2Se3,[17] simple two terminal devices could realize the memory function through the polarization dependent diode effect as shown in Fig. 7b, c, d. Different with CIPS heterostructure, the electric transport of α-In_2Se_3 device not only could be determined by the OOP polarization (Fig. 7d), but also by the IP polarization (Fig. 7c). In addition, it is visible light sensitive due to the suitable band gap of ~1.4 eV (Fig. 7c). Ferroelectrics with a narrow band gap are desirable for photovoltaic but rare in nature for traditional ferroelectric ceramic oxides[116–118] and ferroelectric simple binary oxide such as HfO_2/ZrO_2. 2D ferroelectrics such as SnTe (band gap ~1.6 eV for 1 L) and In_2Se_3 has a tunable band gap dependent on the layer number, which could potentially being used as light sensor, energy conversion devices, or energy harvesters in future. Generally, it is also plausible to realize a FeFET-like memory by using 2D ferroelectric materials, which has been successfully demonstrated in a doped HfO_2 FeFET structure fabricated using a 28 nm technology.[119] The advantage of HfO_2 includes the good silicon compatibility and the large polarization (~40 μC/cm^2). These outstanding features make HfO_2 a promising materials for future non-volatile memories. Different with HfO_2 and traditional perovskite ferroelectrics which are usually wide band gap insulators, most 2D ferroelectrics, theoretically predicted or experimental reported, are semiconducting with moderate band gaps, making it possible to achieve the FeFET-like device without using additional semiconducting channel layer, so as to improve the device integration and the memory density. However, there is a long way to go in order to achieve this goal, considering the small out-of-plane polarization value for 2D ferroelectrics (e.g., ~3.8 μC/cm^2 for CIPS[13]) and the difficulty in large area production of 2D ferroelectrics.

CONCLUSIONS

Although diverse 2D materials have been predicted to possess intrinsic piezoelectricity, most of them, like SnS and GaSe, are not yet investigated experimentally owing to the huge difficulties in materials preparations using exfoliation or CVD methods. For 2D piezoelectric materials, the efforts for future fundamental research or industrial applications may be made in the following aspects: (1) the influence of strain on electronic structure of piezoelectric 2D materials should be thoroughly investigated because the piezoelectric charges can affect the related quantum yield; (2) controlled synthesis of 2D piezoelectric materials with ideal and uniform carrier concentrations, which is very important for the improvement of piezoelectric output (coefficient); and (3) seeking more stable 2D piezoelectric materials that can be chemically stable in the ambient environment. Compared with traditional ferroelectric ceramics, 2D ferroelectrics have shown advantages, such as band gap tenability and flexibility, promising its applications as electronic sensors and data memories. The research of 2D ferroelectric however is still in its infancy stage. To promote the research, further works need to be done especially in the following aspects: (1) the quantitative characterization of 2D ferroelectricity. i.e., to determine the exact polarization value, the Curie temperature, and the piezoelectric coefficient. (2). To understand the special domain patterns and its evolution under the external electric field. (3). To fabricate high-quality 2D ferroelectrics in a large scale with low costs.

ACKNOWLEDGEMENTS

C.J.C. thanks the support from Tsinghua University. W.J.H thanks the support from the "Hundred Talents Program" of the Chinese Academy of Sciences. L.J.L. acknowledges the support from King Abdullah University of Science and Technology (KAUST).

AUTHOR CONTRIBUTIONS

L.J.L. directed the project. C.J.C. and W.J.H drafted section 1 and section 2. F.X. and W. J.H. drafted section 3 and section 4 separately. Section 5 was drafted by C.J.C., F.X., and W.J.H. together. All authors discussed and modified the manuscript at all stages. C.J.C. and F.X. contributed equally to this work.

ADDITIONAL INFORMATION

Competing interests: The authors declare no competing interests.

Publisher's note Springer Nature remains neutral with regard to jurisdictional claims in published maps and institutional affiliations.

REFERENCES

1. Novoselov, K. S. et al. Electric field effect in atomically thin carbon films. *Science* **306**, 666 (2004).
2. Radisavljevic, B., Radenovic, A., Brivio, J., Giacometti, V. & Kis, A. Single-layer MoS_2 transistors. *Nat. Nanotechnol.* **6**, 147 (2011).
3. Lopezsanchez, O., Lembke, D., Kayci, M., Radenovic, A. & Kis, A. Ultrasensitive photodetectors based on monolayer MoS_2. *Nat. Nanotechnol.* **8**, 497 (2013).
4. Zeng, H., Dai, J., Yao, W., Xiao, D. & Cui, X. Valley polarization in MoS_2 monolayers by optical pumping. *Nat. Nanotechnol.* **7**, 490 (2012).
5. Cong, C. et al. Synthesis and optical properties of large-area single-crystalline 2D semiconductor WS_2 monolayer from chemical vapor deposition. *Adv. Opt. Mater.* **2**, 131–136 (2014).
6. Bertolazzi, S., Brivio, J. & Kis, A. Stretching and breaking of ultrathin MoS_2. *ACS Nano* **5**, 9703 (2011).
7. Cai, Y., Lan, J., Zhang, G. & Zhang, Y. W. Lattice vibrational modes and phonon thermal conductivity of monolayer MoS_2. *Phys. Rev. B* **89**, 035438 (2014).
8. Chhowalla, M. et al. The chemistry of two-dimensional layered transition metal dichalcogenide nanosheets. *Nat. Chem.* **5**, 263–275 (2013).
9. Wu, W. et al. Piezoelectricity of single-atomic-layer MoS_2 for energy conversion and piezotronics. *Nature* **514**, 470 (2014).
10. Duerloo, K. A. N., Ong, M. T. & Reed, E. J. Intrinsic piezoelectricity in two-dimensional materials. *J. Phys. Chem. Lett.* **3**, 2871–2876 (2012).
11. Chang, K. et al. Discovery of robust in-plane ferroelectricity in atomic-thick SnTe. *Science* **353**, 274 (2016).
12. Maisonneuve, V., Cajipe, V. B., Simon, A., Muhll, R. V. D. & Ravez, J. Ferrielectric ordering in lamellar $CuInP_2S_6$. *Phys. Rev. B* **56**, 10860–10868 (1997).
13. Liu, F. et al. Room-temperature ferroelectricity in $CuInP_2S_6$ ultrathin flakes. *Nat. Commun.* **7**, 12357 (2016).
14. Ding, W. et al. Prediction of intrinsic two-dimensional ferroelectrics in In_2Se_3 and other III2-VI3 van der Waals materials. *Nat. Commun.* **8**, 14956 (2017).
15. Fei, R., Kang, W. & Yang, L. Ferroelectricity and phase transitions in monolayer group-IV monochalcogenides. *Phys. Rev.Lett.* **117**, 097601 (2016).
16. Bune, A. V. et al. Two-dimensional ferroelectric films. *Nature* **391**, 874–877 (1998).
17. Cui, C. et al. Intercorrelated in-plane and out-of-plane ferroelectricity in ultrathin two-dimensional layered semiconductor In_2Se_3. *Nano Lett.* **18**, 1253–1258 (2018).
18. Fei, R., Li, W., Li, J. & Yang, L. Giant piezoelectricity of monolayer group IV monochalcogenides: SnSe, SnS, GeSe, and GeS. *Appl. Phys. Lett.* **107**, 043001–043237 (2015).
19. Hu, T. & Dong, J. Two new phases of monolayer group-IV monochalcogenides and their piezoelectric properties. *Phys. Chem. Chem. Phys.* **18**, 32514–32520 (2016).
20. Sahin, H. et al. Monolayer honeycomb structures of group IV elements and III-V binary compounds. *Phys. Rev. B* **80**, 155453 (2009).

21. Blonsky, M. N., Zhuang, H. L., Singh, A. K. & Hennig, R. G. Ab Initio prediction of piezoelectricity in two-dimensional materials. *Acs Nano* **9**, 9885–9891 (2015).
22. Gao, R. & Gao, Y. Piezoelectricity in two-dimensional group III-V buckled honeycomb monolayers. *Phys. Status Solidi (RRL)-R. Res. Lett.* **11**, 1600412 (2017).
23. Michel, K. H., Çakır, D., Sevik, C. & Peeters, F. M. Piezoelectricity in two-dimensional materials: Comparative study between lattice dynamics and ab initio calculations. *Phys. Rev. B* **95**, 125415 (2017).
24. Ong, M. T., Duerloo, K. A. N. & Reed, E. J. The effect of hydrogen and fluorine coadsorption on the piezoelectric properties of graphene. *J. Phys. Chem. C.* **117**, 3615–3620 (2012).
25. Chang, Z., Yan, W., Shang, J. & Liu, J. Z. Piezoelectric properties of graphene oxide: A first-principles computational study. *Appl. Phys. Lett.* **105**, 023103–023105 (2014).
26. Sevik, C., Çakır, D., Gülseren, O. & Peeters, F. M. Peculiar piezoelectric properties of soft two-dimensional materials. *J. Phys. Chem. C.* **120**, 13948–13953 (2016).
27. Chandrasekaran, A., Mishra, A. & Singh, A. K. Ferroelectricity, antiferroelectricity, and ultrathin 2D electron/hole gas in multifunctional monolayer MXene. *Nano Lett.* **17**, 3290 (2017).
28. Belianinov, A. et al. $CuInP_2S_6$-room temperature layered ferroelectric. *Nano Lett.* **15**, 3808–3814 (2015).
29. Novoselov, K. S., Jiang, D., Schedin, F., Booth, T. J., Khotkevich, V. V., Morozov, S. V., & Geim, A. K. Two-dimensional atomic crystals. *Proc. Natl Acad. Sci. USA* **102**, 10451–10453 (2005).
30. Coleman, J. N. et al. Two-dimensional nanosheets produced by liquid exfoliation of layered materials. *Science* **42**, 568–571 (2011).
31. Smith, R. J. et al. Large-scale exfoliation of inorganic layered compounds in aqueous surfactant solutions. *Adv. Mater.* **23**, 3944 (2011).
32. Joensen, P., Frindt, R. F., & Morrison, S. R. Single-layer MoS2. *Mater. Res. Bull.* **21**, 457–461 (1986).
33. Rocquefelte, X. et al. Mo cluster formation in the intercalation compound $LiMoS_2$. *Phys. Rev. B* **62**, 2397–2400 (2000).
34. Zeng, Z. et al. Single-layer semiconducting nanosheets: high-yield preparation and device fabrication. *Angew. Chem.* **123**, 11093–11097 (2011).
35. Zeng, Z. et al. An effective method for the fabrication of few-layer-thick inorganic nanosheets. *Angew. Chem.* **124**, 9186–9190 (2012).
36. Eda, G. et al. Photoluminescence from chemically exfoliated MoS_2. *Nano Lett.* **11**, 5111–5116 (2011).
37. Nicolosi, V., Chhowalla, M., Kanatzidis, M. G., Strano, M. S. & Coleman, J. N. Liquid exfoliation of layered materials. *Science* **340**, 1420 (2013).
38. Zhan, Y., Liu, Z., Najmaei, S., Ajayan, P. M. & Lou, J. Large-area vapor-phase growth and characterization of MoS(2) atomic layers on a SiO(2) substrate. *Small* **8**, 966–971 (2012).
39. Liu, K. K. et al. Growth of large-area and highly crystalline MoS_2 thin layers on insulating substrates. *Nano Lett.* **12**, 1538–1544 (2012).
40. Lin, M. et al. Controlled growth of atomically thin In_2Se_3 flakes by van der Waals epitaxy. *J. Am. Chem. Soc.* **135**, 13274 (2013).
41. Zhou, J. et al. Controlled synthesis of high-quality monolayered α-In_2Se_3 via physical vapor deposition. *Nano Lett.* **15**, 6400 (2015).
42. Feng, W. et al. Sensitive electronic-skin strain sensor array based on the patterned two-dimensional α-In_2Se_3. *Chem. Mater.* **28**, (2016).
43. Yu, S. M., Jin, H. Y., Patole, S. P., Lee, J. H. & Yoo, J. B. The effect of pressure and growth temperature on the characteristics of polycrystalline In_2Se_3 films in metal organic chemical vapor deposition. *Electron. Mater. Lett.* **8**, 245–250 (2012).
44. Kalinin, S. V. & Gruverman, A. (eds) Scanning probe microscopy: Electrical and electromechanical phenomenon at the nanoscale. Vol. 1. (Springer, 2007).
45. Zhu, H. et al. Observation of piezoelectricity in free-standing monolayer MoS_2. *Nat. Nanotechnol.* **10**, 151 (2015).
46. Hu, W. J. et al. Universal ferroelectric switching dynamics of vinylidene fluoride-trifluoroethylene copolymer films. *Sci. Rep.* **4**, 4772 (2015).
47. Seol, D., Kim, B. & Kim, Y. Non-piezoelectric effects in piezoresponse force microscopy. *Curr. Appl. Phys.* **17**, 661–674 (2017).
48. Kalinin, S. et al. Li-ion dynamics and reactivity on the nanoscale. *Mater. Today* **14**, 548–558 (2011).
49. Kalinin, S. V., Rar, A. & Jesse, S. A decade of piezoresponse force microscopy: progress, challenges, and opportunities. *IEEE Trans. Ultrason. Ferroelectr. Freq. Control* **53**, 2226–2252 (2006).
50. Gruverman, A., Auciello, O. & Tokumoto, H. Imaging and control of domain structures in ferroelectric thin films via scanning force microscopy. *Annu. Rev. Mater. Res.* **28**, 101–123 (1998).
51. Alexe, M., Gruverman, A., (eds.) Nanoscale characterization of ferroelectric materials. (Springer: Berlin, 2004).
52. Gopalan, V. & Raj, R. Domain structure and phase transitions in epitaxial $KNbO_3$ thin films studied by in situ second harmonic generation measurements. *Appl. Phys. Lett.* **68**, 1323–1325 (1996).
53. Yokota, H., Haumont, R., Kiat, J. M., Matsuura, H. & Uesu, Y. Second harmonic generation microscopic observations of a multiferroic $BiFeO_3$ single crystal. *Appl. Phys. Lett.* **95**, 082904 (2009).
54. Denev, S. A., Lummen, T. T. A., Barnes, E., Kumar, A. & Gopalan, V. Probing ferroelectrics using optical second harmonic generation. *J. Am. Ceram. Soc.* **94**, 2699–2727 (2011).
55. Tenne, D. A. et al. Probing nanoscale ferroelectricity by ultraviolet raman spectroscopy. *Science* **313**, 1614–1616 (2006).
56. Fong, D. D. & Thompson, C. Ferroelectricity in ultrathin perovskite films. *Science* **304**, 1650–1653 (2004).
57. Gao, P. et al. Possible absence of critical thickness and size effect in ultrathin perovskite ferroelectric films. *Nat. Commun.* **8**, 15549 (2017).
58. Masmanidis, S. C. et al. Multifunctional nanomechanical systems via tunably coupled piezoelectric actuation. *Science* **317**, 780 (2007).
59. Kingon, A. I. & Srinivasan, S. Lead zirconate titanate thin films directly on copper electrodes for ferroelectric, dielectric and piezoelectric applications. *Nat. Mater.* **4**, 233–237 (2005).
60. Wang, Z. L. & Song, J. Piezoelectric nanogenerators based on Zinc Oxide nanowire arrays. *Science* **312**, 242 (2006).
61. Safari, A. & Akdogan, E. K. *Piezoelectric and acoustic materials for transducer applications*. (Springer-Verlag, US, 2008).
62. Wang, Q. H., Kalantar-Zadeh, K., Kis, A., Coleman, J. N. & Strano, M. S. Electronics and optoelectronics of two-dimensional transition metal dichalcogenides. *Nat. Nanotechnol.* **7**, 699–712 (2012).
63. Ganatra, R. & Zhang, Q. Few-layer MoS_2: a promising layered semiconductor. *Acs Nano* **8**, 4074 (2014).
64. Kim, S. K. et al. Directional dependent piezoelectric effect in CVD grown monolayer MoS_2 for flexible piezoelectric nanogenerators. *Nano Energy* **22**, 483–489 (2016).
65. Lee, J. H. et al. Reliable piezoelectricity in bilayer WSe_2 for piezoelectric nanogenerators. *Adv. Mater.* **29**, 1606667 (2017).
66. Qi, J. et al. Piezoelectric effect in chemical vapour deposition-grown atomic-monolayer triangular molybdenum disulfide piezotronics. *Nat. Commun.* **6**, 7430 (2015).
67. Michel, K. H. & Verberck, B. Theory of elastic and piezoelectric effects in two-dimensional hexagonal boron nitride. *Phys. Rev. B Condens. Matter* **80**, 308–310 (2009).
68. Li, Y. et al. Probing symmetry properties of few-layer MoS_2 and h-BN by optical second-harmonic generation. *Nano Lett.* **13**, 3329–3333 (2013).
69. Zelisko, M. et al. Anomalous piezoelectricity in two-dimensional graphene nitride nanosheets. *Nat. Commun.* **5**, 4284 (2014).
70. Li, W. & Li, J. Piezoelectricity in two-dimensional group-III monochalcogenides. *Nano Res.* **8**, 3796–3802 (2015).
71. Y, Z. et al. Out-of-plane piezoelectricity and ferroelectricity in layered α-In_2Se_3 nanoflakes. *Nano Lett.* **17**, 5508 (2017).
72. Da, C. R. G. et al. Strong piezoelectricity in single-layer graphene deposited on SiO_2 grating substrates. *Nat. Commun.* **6**, 7572 (2015).
73. Jin, H. J., Yoon, W. Y. & Jo, W. Virtual out-of-plane piezoelectric response in MoS_2 layers controlled by ferroelectric polarization. *ACS Appl. Mater. Inter.* **10**, 1334–1339 (2017).
74. Lu, A. Y. et al. Janus monolayers of transition metal dichalcogenides. *Nat. Nanotechnol.* **12**, 744 (2017).
75. Wang, X. et al. Subatomic deformation driven by vertical piezoelectricity from CdS ultrathin films. *Sci. Adv.* **2**, e1600209–e1600209 (2016).
76. Wu, W., Wen, X. & Wang, Z. L. Taxel-addressable matrix of vertical-nanowire piezotronic transistors for active and adaptive tactile imaging. *Science* **340**, 952 (2013).
77. Xue, F. et al. Influence of external electric field on piezotronic effect in ZnO nanowires. *Nano Res.* **8**, 2390–2399 (2015).
78. Pradel, K. C. et al. Piezotronic effect in solution-grown p-type ZnO nanowires and films. *Nano Lett.* **13**, 2647 (2013).
79. Xue, F. et al. p-type MoS_2 and n-type ZnO diode and its performance enhancement by the piezophototronic effect. *Adv. Mater.* **28**, 3391 (2016).
80. Xue, F. et al. Enhanced photoresponsivity of the MoS_2-GaN heterojunction diode via the piezo-phototronic effect. *NPG Asia Mater.* **9**, e418 (2017).
81. Pan, C. et al. High-resolution electroluminescent imaging of pressure distribution using a piezoelectric nanowire LED array. *Nat. Photon.* **7**, 752–758 (2013).
82. Wu, W. et al. Piezophototronic effect in single-atomic-layer MoS_2 for strain-gated flexible optoelectronics. *Adv. Mater.* **28**, 8463 (2016).
83. Rezk, A. R. et al. Acoustically-driven trion and exciton modulation in piezoelectric two-dimensional MoS_2. *Nano Lett.* **16**, 849 (2016).
84. Tsymbal, E. Y. & Kohlstedt, H. Tunneling across a Ferroelectric. *Science* **313**, 181–183 (2006).
85. Kaminow, I. P. *Principles and applications of ferroelectrics and related materials*. (Clarendon, Oxford, 1977).

86. Zhong, W. L., Wang, Y. G., Zhang, P. L. & Qu, B. D. Phenomenological study of the size effect on phase transition in ferroelectric particles. *Phys. Rev. B Condens. Matter* **50**, 698–703 (1994).
87. Junquera, J. & Ghosez, P. Critical thickness for ferroelectricity in perovskite ultrathin films. *Nature* **422**, 506–509 (2003).
88. Lichtensteiger, C., Triscone, J. M., Junquera, J. & Ghosez, P. Ferroelectricity and tetragonality in ultrathin $PbTiO_3$ films. *Phys. Rev. Lett.* **94**, 047603 (2005).
89. Gruverman, A. et al. Tunneling electroresistance effect in ferroelectric tunnel junctions at the nanoscale. *Nano Lett.* **9**, 3539 (2009).
90. Wei, J. H., Wang, Z., Yu, W. & Wu, T. Optically controlled electroresistance and electrically controlled photovoltage in ferroelectric tunnel junctions. *Nat. Commun.* **7**, 10808 (2016).
91. Lee, D. et al. Emergence of room-temperature ferroelectricity at reduced dimensions. *Science* **349**, 1314 (2015).
92. Zubko, P., Gariglio, S., Gabay, M., Ghosez, P. & Triscone, J. M. Interface physics in complex oxide heterostructures. *Annu. Rev. Condens. Matter Phys.* **2**, 141–165 (2011).
93. Boscke, T. S., Muller, J., Brauhaus, D., Schroder, U. & Bottger, U. Ferroelectricity in hafnium oxide thin films. *Appl. Phys. Lett.* **99**, 102903 (2011).
94. Müller, J. et al. Ferroelectricity in simply binary ZrO_2 and HfO_2. *Nano Lett.* **12**, 4318–4323 (2012).
95. Schroeder, U. et al. Impact of different dopants on the switching properties of ferroelectric hafniumoxide. *Jpn. J. Appl. Phys.* **53**, 08LE02 (2014).
96. Chernikova, A. et al. Ultrathin $Hf_{0.5}Zr_{0.5}O_2$ ferroelectric films on Si. *ACS Appl. Mater. Inter.* **8**, 7232–7237 (2016).
97. Schroeder, U., Slesazeck, S., Mikolajick, T. Nonvolatile Field-Effect Transistors Using Ferroelectric Doped HfO_2 Films in *Ferroelectric-gate field effect transistor memories: Device physics and applications* (eds Park, B. E., Ishiwara, H., Okuyama, M., Sakai, S., & Yoon, S. M.) Ch. 3 (Springer, Berlin, 2016).
98. Schenk, T. et al. About the deformation of ferroelectric hystereses. *Appl. Phys. Rev.* **1**, 041103 (2014).
99. Li, X. et al. Large-area synthesis of high-quality and uniform graphene films on copper foils. *Science* **324**, 1312 (2009).
100. Keum, D. H. et al. Bandgap opening in few-layered monoclinic $MoTe_2$. *Nat. Phys* **11**, 482–486 (2015).
101. Shirodkar, S. N. & Waghmare, U. V. Emergence of ferroelectricity at a metal-semiconductor transition in a 1T monolayer of MoS_2. *Phys. Rev. Lett.* **112**, 157601 (2014).
102. Sante, D. D., Stroppa, A., Barone, P., Whangbo, M. H. & Picozzi, S. Emergence of ferroelectricity and spin-valley properties in two-dimensional honeycomb binary compounds. *Phys. Rev. B* **91**, 161401 (2015).
103. Luo, W. & Xiang, H. Two-dimensional phosphorus oxides as energy and information materials. *Angew. Chem. Int. Ed.* **55**, 8575–8580 (2016).
104. Stengel, M., Vanderbilt, D. & Spaldin, N. A. Enhancement of ferroelectricity at metal-oxide interfaces. *Nat. Mater.* **8**, 392–397 (2009).
105. Iizumi, M., Hamaguchi, Y., Komatsubara, K. F. & Kato, Y. Phase transition in SnTe with low carrier concentration. *J. Phys. Soc. Jpn.* **38**, 443–449 (1975).
106. Rodriguez, B. J., Callahan, C., Kalinin, S. V. & Proksch, R. Dual-frequency resonance-tracking atomic force microscopy. *Nanotechnology* **18**, 162–193 (2007).
107. Hellwege, K. H., Hellwege, A. M. Ferroelectrics and related substances: Oxides. (Landolt-Bornstein, New Series, Group III, Vol. 36A, 1989).
108. Ye, J., Soeda, S., Nakamura, Y. & Nittono, O. Crystal structures and phase transformation in In_2Se_3 compound semiconductor. *Jpn. J. Appl. Phys.* **37**, 4264–4271 (1998).
109. Cruz, M. P. et al. Strain control of domain-wall stability in epitaxial $BiFeO_3$ (110) films. *Phys. Rev. Lett.* **99**, 217601 (2007).
110. Scott, J. F. Applications of modern ferroelectrics. *Science* **315**, 954–959 (2007).
111. Jeong, D. S. et al. Emerging memories: resistive switching mechanisms and current status. *Rep. Prog. Phys. Phys. Soc.* **75**, 076502 (2012).
112. Blom, P. W. M., Wolf, R. M., Cillessen, J. F. M., Krijn, M. P. C. P. Ferroelectric Schottky diode. *Phys. Rev. Lett.* **73**, 2107 (1994).
113. Yi, H. T., Choi, T., Choi, S. G., Oh, Y. S. & Cheong, S. W. Mechanism of the switchable photovoltaic effect in ferroelectric $BiFeO_3$. *Adv. Mater.* **23**, 3403 (2011).
114. Kohlstedt, H., Pertsev, N. A., Contreras, J. R. & Waser, R. Theoretical current-voltage characteristics of ferroelectric tunnel junctions. *Physics* **72**, 125341 (2005).
115. Zhuravlev, M. Ye, S., R. F., Jaswal, S. S. & Tsymbal, E. Y. Giant electroresistance in ferroelectric tunnel junctions. *Phys. Rev. Lett.* **94**, 4 (2005).
116. Berglund, C. N. & Braun, H. J. Optical absorption in single-domain ferroelectric barium titanate. *Phys. Rev.* **164**, 790–799 (1967).
117. Dhar, A. & Mansingh, A. Optical properties of reduced lithium niobate single crystals. *J. Appl. Phys.* **68**, 5804–5809 (1990).
118. Jiang, Y. P., Tang, X. G., Liu, Q. X., Li, Q. & Ding, A. L. Optical properties of Pb $(Zr_{0.53}Ti_{0.47})O_3$ thin films on Pt-coated Si substrates measured by spectroscopic ellipsometry in the UV–vis–NIR region. *Mater. Sci. Eng. B* **137**, 304–309 (2007).
119. Yurchuk, E. et al. Impact of scaling on the performance of HfO_2-based ferroelectric field effect transistors. *IEEE Trans. Electron Dev.* **61**, 3699–3706 (2014).

Open Access This article is licensed under a Creative Commons Attribution 4.0 International License, which permits use, sharing, adaptation, distribution and reproduction in any medium or format, as long as you give appropriate credit to the original author(s) and the source, provide a link to the Creative Commons license, and indicate if changes were made. The images or other third party material in this article are included in the article's Creative Commons license, unless indicated otherwise in a credit line to the material. If material is not included in the article's Creative Commons license and your intended use is not permitted by statutory regulation or exceeds the permitted use, you will need to obtain permission directly from the copyright holder. To view a copy of this license, visit http://creativecommons.org/licenses/by/4.0/.

© The Author(s) 2018